Phonon-Broadened Impurity Spectra. I. Density of States

C. B. DUKE AND G. D. MAHAN
General Electric Research Laboratory, Schenectady, New York
(Received 28 April 1965)

The phonon-broadened densities of states associated with (a) a point charge, (b) an S-wave hydrogenic shallow donor, and (c) an exciton bound to a neutral defect are calculated. The electronic states are coupled to the lattice vibrations via the (a) longitudinal-optical, (b) piezoelectric, and (c) deformation-potential linear electron-phonon interactions. The major dynamical approximations consist of the use of the Debye model for the acoustical-phonon spectrum and the neglect of the mixing of electronic states by phonons. Within the framework of the model Hamiltonian the Fourier transforms of the densities of states are calculated exactly and analytically. For CdS, CdTe, and ZnS numerical calculations of the densities of states are presented. The density of states associated with a shallow donor in CdTe and ZnS exhibits, in lieu of a zero-phonon line, a Lorentzian peak whose width is proportional to temperature. The inclusion of the static shielding of the piezoelectric interaction by mobile charge carriers replaces the Lorentzian by a zero-phonon line plus two shoulders. The extensions of the calculation to donor-acceptor, band-impurity, interband, and intra-deep-impurity transitions are discussed.

I. INTRODUCTION

IN this paper we calculate the modification of the density of states associated with a localized electron in a crystal due to its interaction with lattice vibrations via (a) optical, (b) piezoelectric, and (c) deformation-potential electron-phonon coupling. The results are well known for the case in which the electron couples to longitudinal-optical phonons.[1,2] They are rederived herein primarily to facilitate the comparison of our results and notation to others in the literature. The coupling of the electron to piezoelectric phonons is considered both with and without the static shielding of the interaction by mobile charge carriers. Hopfield[3] discussed the latter situation for an exciton bound to a neutral defect. Our results for this case are more general than his. Using the same dynamical approximations in the Hamiltonian we obtain the spectral function exactly whereas he relied on an iterative expansion of it. The coupling of an electronic state to phonons via the deformation potential has also been considered by other authors.[4–6] The results presented herein differ from theirs in that within the framework of a simplified Hamiltonian we calculate the spectral function without relying on further calculational approximations or the use of perturbation theory.

Our major dynamical approximation consists of the use of the Debye model with an average speed of sound for the acoustical-phonon excitation spectrum. This approximation is made primarily because it permits the Fourier transform of the one-electron spectral function to be evaluated exactly. Although frequently employed, the approximation has two major consequences. First, the changes in the normal-mode spectrum due to the presence of the impurity are neglected. For example, effects due to the local modes associated with light impurities[7] and alterations in the short-wavelength density of (phonon) states associated with the heavy impurities[8] are neglected. Second, peaks in the (electron) spectral function due to critical points in the phonon spectra are not accounted for by a Debye spectrum.[9] Therefore our model is suitable for describing the line shape of narrow phonon-broadened spectral lines in solids due either to electronic transitions at a point defect or to sharp-line pair recombination radiation such as that observed in GaP.[10] For these narrow lines, the above modifications of the phonon spectra only cause discernible effects in the one-electron spectral function at energies associated with the Brillouin-zone boundaries. However, these effects do not alter our main conclusions.

The second dynamical approximation consists of the pair of assumptions that the electron-phonon interaction is linear and that the phonons do not mix different electronic states. The latter approximation is expected to be quite accurate for transitions between nondegenerate localized electronic states. These localized states are usually separated by energies much larger

[1] K. Huang and A. Rhys, Proc. Roy. Soc. (London) **A204**, 406 (1950).
[2] J. J. Markham, Rev. Mod. Phys. **31**, 956 (1959), has reviewed the literature on the interaction of localized electrons with longitudinal-optical phonons.
[3] J. J. Hopfield, *Proceedings of the International Conference on the Physics of Semiconductors, Exeter, 1962* (The Institute of Physics and the Physical Society, London, England, 1962), p. 75.
[4] E. O. Kane, Phys. Rev. **119**, 40 (1960).
[5] D. E. McCumber and M. D. Sturge, J. Appl. Phys. **34**, 1682 (1963); D. E. McCumber, J. Math. Phys. **5**, 222 (1964); G. F. Imbusch, W. M. Yen, A. L. Schawlow, D. E. McCumber, and M. D. Sturge, Phys. Rev. **133**, A1029 (1964); and B. DiBartolo and R. Peccei, *ibid.* **137**, A 1770 (1965).
[6] A body of literature on the wave functions of trapped electrons in crystals also contains discussions of LO and deformation-potential electron-phonon interactions. See, e.g., B. S. Gourary and F. J. Adrian, Solid State Phys. **10**, 127 (1960).
[7] See, e.g., G. Schaefer, J. Phys. Chem. Solids **12**, 233 (1960); M. Balkanski and W. Nazarewicz, *ibid.* **25**, 437 (1964).
[8] See, e.g., P. G. Dawber and R. J. Elliot, Proc. Phys. Soc. (London) **81**, 453 (1963).
[9] See, e.g., C. B. Pierce, Phys. Rev. **135**, A83 (1964); D. Langer and S. Ibuki, *ibid.* **138**, A809 (1965).
[10] J. J. Hopfield, D. G. Thomas, and M. Gershenzon, Phys. Rev. Letters **10**, 162 (1963); D. G. Thomas, M. Gershenzon, and F. A. Trumbore, Phys. Rev. **133**, A269 (1964).

than the Debye energy so that all mixing effects are second or higher order in the electron-phonon interaction. In particular, this approximation ignores the temperature-dependent polaron shift and lifetime broadening of the zero-phonon line.[5] However, we obtain additional structure near the zero-phonon line which scales linearly in the temperature as opposed to the T^4 and T^7 low-temperature scaling of the polaron shift and lifetime broadening, respectively. The neglect of electronic-state mixing by phonons *a priori* limits the direct applicability of the analysis to transitions between localized states.

Within the framework of the above two approximations our evaluation of the one-electron density of states (spectral function) is exact for charges well localized relative to a lattice spacing. For electron states which are extended relative to a lattice spacing we use in addition the effective-mass method of Kohn[11] and neglect Brillouin-zone edge effects. However, no iterative approximations or moment expansions are employed. The Fourier transforms of the spectral functions are calculated analytically and exactly, with the final Fourier transformation being performed by numerical integration. Where a zero-phonon line is present, we derive an exact analytical formula for its spectral weight as a function of temperature and other relevant parameters.

In this paper we present only the analytical and sample numerical results. In Sec. II we specify our Hamiltonian and give the general formulas for the spectral function. In Sec. III the interaction of an arbitrary electronic state with longitudinal-optical (LO) phonons is discussed. We present in Sec. IV the analysis of a point charge interacting with Debye phonons via an unshielded piezoelectric electron-phonon interaction. The next topic to be discussed is the interaction of phonons with a shallow impurity state possessing a hydrogenic S-wave envelope function. In Sec. V the interaction is considered to occur via the unshielded piezoelectric and deformation-potential interactions. In Sec. VI the modification of these results due to the shielding of the piezophonon interaction by mobile charge carriers is given. In Sec. VII we present an analysis of the exciton bound to a neutral impurity analogous to that of Hopfield.[3] A synopsis of the results is given in Sec. VIII.

II. DEFINITION OF THE BOUNDARY-VALUE PROBLEM

The general Hamiltonian for a coupled electron-phonon system interacting via a linear interaction is given, in the notation of second quantization, by

$$H=\sum_\lambda E_\lambda c_\lambda^\dagger c_\lambda+\sum_{\mathbf{k}} \hbar\omega(\mathbf{k}) \times[a_{\mathbf{k}}^\dagger a_{\mathbf{k}}+\tfrac{1}{2}]+\sum_{\mathbf{k}} V_{\mathbf{k}}[a_{\mathbf{k}}\rho(-\mathbf{k})+a_{\mathbf{k}}^\dagger\rho(\mathbf{k})], \quad (2.1)$$

$$\rho(\mathbf{k})=\sum_{\lambda',\lambda} c_{\lambda'}^\dagger c_\lambda M_{\lambda',\lambda}(\mathbf{k}), \quad (2.2a)$$

$$M_{\lambda',\lambda}(\mathbf{k})=\int d^3x e^{-i\mathbf{k}\cdot\mathbf{x}}\tilde{\phi}_{\lambda'}(\mathbf{x})\phi_\lambda(\mathbf{x}). \quad (2.2b)$$

The electrons alone are taken to have eigenfunctions $\phi_\lambda(\mathbf{x})$ with associated eigenvalues E_λ and creation operators $c_\lambda^\dagger$. The phonons are labeled by the quasi-momentum $\mathbf{k}$ (we suppress polarization indices) and have the energy spectrum $\hbar\omega(\mathbf{k})$. The phonon creation operator is $a_{\mathbf{k}}^\dagger$. The electron-phonon interaction is denoted by $V_{\mathbf{k}}$. We confine our attention to systems which are optically isotropic. Cubic crystals rigorously exhibit optical isotropy and the anisotropy in the dielectric function is often neglected in the treatment of piezoelectric modes in Wurtzite structures.[12,13]

The Hamiltonian is simplified by use of the two dynamical approximations discussed in the Introduction. The acoustical phonon spectrum is taken to be a Debye spectrum

$$\omega(\mathbf{k})=v_s k; \quad k\leq(6\pi^2 n_0)^{1/3}, \quad (2.3)$$

in which n_0 is the number of atoms per cm^{+3} in the crystal. We further neglect the difference in the sound velocity between longitudinal and shear modes by using an average velocity of sound in (2.3). Denoting the density of the crystal by ρ_0, for zincblende structures we use the value obtained from

$$\frac{1}{v_s^2}=\frac{\rho_0}{13}\left[\frac{4}{C_{44}}+\frac{1}{C_{11}}+\frac{4}{C_{11}-C_{12}}+\frac{4}{C_{11}+C_{12}+2C_{44}}+\frac{4}{C_{11}+2C_{12}+4C_{44}}+\frac{8}{C_{11}-C_{12}+C_{44}}\right], \quad (2.4)$$

which emphasizes the contribution of the shear modes. In treatments of electronic mobilities in piezoelectric crystals,[12–14] the velocity average is usually taken within the framework of calculating an average electromechanical coupling constant. For cubic structures this procedure is equivalent to using an average velocity of sound. Therefore as any of the averaging procedures yield results deviating from the exact ones by factors ≈ 1, for cubic structures we embody all of our averaging in (2.4) alone. For Wurtzite structures we use the averaging procedure of Hutson.[12]

The equality of the longitudinal and transverse sound velocities would result (in a cubic structure) if the relations

$$C_{11}=C_{12}+2C_{44} \text{ (elastic isotropy)}, \quad (2.5a)$$

[11] W. Kohn, Solid State Phys. **5**, 258 (1957).

[12] A. R. Hutson, J. Appl. Phys. Suppl. **32**, 2287 (1961).

[13] J. D. Zook, Phys. Rev. **136**, A869 (1964). The approximation is implicit (although not explicitly stated) in Eq. (4) of this reference.

[14] H. J. G. Meijer and D. Polder, Physica **19**, 225 (1953); and W. A. Harrison, University of Illinois, Ph.D. thesis, 1956 (unpublished); Phys. Rev. **101**, 903 (1956).

$C_{12}=-C_{44}$

(longitudinal-transverse degeneracy), (2.5b)

were satisfied. A tractable model of a cubic piezoelectric material is obtained by assuming relations (2.5) and using (2.4) to calculate the common speed of sound. For this model Eq. (2.10c) gives the electron-piezophonon interaction and the calculation of the one-electron spectral functions can be carried through easily and explicitly for arbitrary charge distributions. All of the numerical calculations on zincblende structures are performed within the framework of this model.

The dispersion relation for the longitudinal-optical modes is taken to be that given by the Lyddane-Sachs-Teller relation[15]

$$\omega(\mathbf{k})=\omega_l=[\epsilon(0)/\epsilon(\infty)]^{1/2}\omega_0, \tag{2.6}$$

in which $\epsilon(0)$ is the static dielectric constant, $\epsilon(\infty)$ is the "high-frequency" dielectric constant, and ω_0 is the reststrahl frequency.

The second dynamical approximation is the neglect of off-diagonal matrix elements of the electron density operator (2.2). It reduces Eq. (2.1) to the form

$$H=\sum_\lambda E_\lambda c_\lambda^\dagger c_\lambda+\sum_{\mathbf{k}}\hbar\omega(\mathbf{k})[a_{\mathbf{k}}^\dagger a_{\mathbf{k}}+\tfrac{1}{2}]+\sum_{\lambda,\mathbf{k}} c_\lambda^\dagger c_\lambda[v(\mathbf{k},\lambda)a_{\mathbf{k}}+v(\mathbf{k},\lambda)^* a_{\mathbf{k}}^\dagger], \tag{2.7a}$$

$$v(\mathbf{k},\lambda)=V_{\mathbf{k}}M_{\lambda,\lambda}(\mathbf{k}). \tag{2.7b}$$

Equations (2.7) are valid only for localized electronic states. An analog of the above analysis for continuum states is obtained by first making the Lee-Low-Pines[16] elimination of the electron's coordinates and subsequently using Van Haeringen's[17] truncation of the resulting Hamiltonian. The final one-electron eigenvalues contain phonon frequencies which explicitly depend on the electron's momentum and effective mass in the initial and final states. Therefore, the formulas analogous to those given below, although they can be derived, are intractable.

The dynamical approximations concerning the phonon spectra alter Eqs. (2.7) both in the free-phonon term and in the electron-phonon vertex $V_{\mathbf{k}}$. Using the adiabatic approximation for the shielding of the piezoelectric electron-phonon interaction by mobile charge carriers, we obtain for the electron-phonon vertex functions:

Optical coupling:

$$V_{\mathbf{k}}=\frac{4\pi q}{k}\left(\frac{\hbar f}{2\Omega\omega_l}\right)^{1/2}, \tag{2.8a}$$

$$f=\frac{\omega_l^2}{4\pi}\left[\frac{1}{\epsilon(0)}-\frac{1}{\epsilon(\infty)}\right]. \tag{2.8b}$$

Deformation-potential coupling:

$$V_{\mathbf{k}}=iD_0[\hbar k/2\Omega\rho_0 v_s]^{1/2}. \tag{2.9}$$

Piezoelectric coupling without screening:

$$V_{\mathbf{k}}=\hbar v_s[2\pi g/k\Omega]^{1/2}, \tag{2.10a}$$

$$g=\pi C_0^2\frac{q^2}{\epsilon(0)\hbar v_s}\frac{e^2}{\epsilon(0)\rho_0 v_s^2}. \tag{2.10b}$$

Piezoelectric coupling with screening:

$$V_{\mathbf{k}}=\hbar v_s[2\pi g/k\Omega]^{1/2}k^2/(k^2+k_D^2), \tag{2.11a}$$

$$k_D^2=4\pi n_q q^2/[\theta\epsilon(0)]. \tag{2.11b}$$

We use the notation q for the charge on the electron, D_0 for the deformation-potential constant (assumed to be associated with a nondegenerate band), Ω for the volume of the system, $\epsilon(\omega)$ for the dielectric function at the angular frequency ω, e for an appropriately averaged piezoelectric constant, C_0 for a numerical constant of order unity and depending on the crystal structure, g for a dimensionless electron-piezophonon coupling constant $\theta=\kappa T$, κ for Boltzmann's constant, and n_q for the net number of mobile charge carriers per cm^3. It should be noted that in nondegenerate semiconductors the temperature dependence of k_D is dominated by an exponential dependence of n_q on $1/\theta$.

For zincblende structures the only averaging used is that given by (2.4) for the speed of sound. We use $\epsilon(\omega)=\epsilon_{11}$ and $e=e_{14}$.[18] If we impose the restrictions (2.5) and calculate v_s from (2.4), then in the principal-axis coordinate system the electron-piezophonon vertex function is given by

$$V_{\mathbf{k}}=\frac{4\pi q}{\epsilon_{11}(0)}e_{14}(\hbar/2\rho_0 v_s k\Omega)^{1/2}\times\left[\frac{k_1^2k_2^2+k_1^2k_3^2+k_2^2k_3^2}{k^4}\right]^{1/2}. \tag{2.10c}$$

The use of Eq. (2.10c) leads to the value of C_0

$$C_0=(4/5)^{1/2} \tag{2.11}$$

for an isotropic charge distribution. In Wurtzite structures we use Hutson's[12] averaging procedure. By employing this procedure we neglect the dielectric and elastic anisotropy while taking separate averages over the three independent piezoelectric constants for longitudinal and transverse elastic waves.

It is well known that (2.7) can be diagonalized.[1] We use the method of canonical transformations with the appropriate transformation, $\exp(iS)$, being given by

$$S=\sum_\lambda S_\lambda, \tag{2.12a}$$

$$S_\lambda=ic_\lambda^\dagger c_\lambda\sum_{\mathbf{k}}\{[v(\mathbf{k},\lambda)a_{\mathbf{k}}-v(\mathbf{k},\lambda)^* a_{\mathbf{k}}^\dagger]/\hbar\omega(\mathbf{k})\}. \tag{2.12b}$$

[15] R. H. Lyddane, R. G. Sachs, and E. Teller, Phys. Rev. **59**, 673 (1941).
[16] T. D. Lee, F. Low, and D. Pines, Phys. Rev. **90**, 297 (1953).
[17] W. Van Haeringen, Phys. Rev. **137**, A1902 (1965).
[18] See, e.g. W. G. Cady, *Piezoelectricity I* (Dover Publications Inc., New York, 1962), p. 192.

The one-electron eigenstates of (2.7) are given by the formulas

$$|\Psi(\lambda,\{n_{\mathbf{k}}\})\rangle=\exp(-iS_\lambda)c_\lambda^\dagger|\{n_{\mathbf{k}}\}\rangle, \quad (2.13a)$$

$$|\{n_{\mathbf{k}}\}\rangle=\prod_{\mathbf{k}}\frac{(a_{\mathbf{k}}^\dagger)^{n_{\mathbf{k}}}}{(n_{\mathbf{k}}!)^{1/2}}|0\rangle, \quad (2.13b)$$

with the corresponding eigenvalues

$$E_\lambda\{n_{\mathbf{k}}\}=E_\lambda-\Delta_\lambda+\sum_{\mathbf{k}}\hbar\omega(\mathbf{k})[n_{\mathbf{k}}+\tfrac{1}{2}], \quad (2.14a)$$

$$\Delta_\lambda=\sum_k[|v(\mathbf{k},\lambda)|^2/\hbar\omega(\mathbf{k})]. \quad (2.14b)$$

Therefore the electron-phonon interaction causes a temperature-independent polaron shift Δ_λ of the one-electron energies and phonon correlations $\exp(-iS_\lambda)|\{n_{\mathbf{k}}\}\rangle$ in the wave function.

We study the density of states associated with the one-electron state given by (2.13a). This state is an eigenstate of (2.7) with the eigenvalue (2.14). However, it is not an eigenstate of the noninteracting electron-phonon Hamiltonian

$$H_0=\sum_\lambda E_\lambda c_\lambda^\dagger c_\lambda+\sum_{\mathbf{k}}\hbar\omega(\mathbf{k})[a_{\mathbf{k}}^\dagger a_{\mathbf{k}}+\tfrac{1}{2}]. \quad (2.15)$$

The utility of a study of the density of states may be seen by considering a dilute concentration of defects in a crystal. The electrons at the defect sites interact simultaneously with local electromagnetic fields in the crystal and with lattice vibrations.[19] In this paper the interaction between defects is ignored. The interaction between the electromagnetic field and the electron is treated in first-order perturbation theory,[2] using as basis states the one-electron eigenstates of Eq. (2.15). The effects of the simultaneous interaction of the electron with lattice vibrations are investigated by asking for the probability $P(\lambda,E)$ that the exact eigenstate (2.13) is an eigenstate of (2.15) with the electron possessing an energy E. At nonzero temperatures the phonons are not in a single eigenstate of (2.15) but rather have a well-defined probability of being in any of their possible eigenstates. Therefore we are led to consider the temperature-dependent probability $P_\beta(\lambda,E)$:

$$P_\beta(\lambda,E)=Z_{\rm ph}^{-1}\sum_{\{n_{\mathbf{k}}'\},\{n_{\mathbf{k}}\}}|\langle\{n_{\mathbf{k}}'\}|c_\lambda|\Psi(\lambda,\{n_{\mathbf{k}}\})\rangle|^2$$
$$\times\exp[-\textstyle\sum_{\mathbf{k}}\beta\hbar\omega(\mathbf{k})(n_{\mathbf{k}}+\frac{1}{2})]\delta$$
$$\times(E+\hbar\textstyle\sum_{\mathbf{k}}\omega(\mathbf{k})[n_{\mathbf{k}}'-n_{\mathbf{k}}]-E_\lambda+\Delta_\lambda), \quad (2.16a)$$

$$Z_{\rm ph}\equiv\sum_{\{n_{\mathbf{k}}\}}\exp[-\beta\hbar\textstyle\sum_{\mathbf{k}}\omega(\mathbf{k})(n_{\mathbf{k}}+\frac{1}{2})], \quad (2.16b)$$

$$\beta=\theta^{-1}. \quad (2.17)$$

[19] For a discussion of a case in which the separation between the electromagnetic and elastic modes of the crystal cannot be made see, e.g., M. Born and K. Huang, *Dynamical Theory of Crystal Lattices* (Clarendon Press, Oxford, England, 1954), p. 89.

The probability $P_\beta(\lambda,E)$ is simply related to the single-hole spectral function[20] and has been recently studied by McCumber.[5] In the single-hole spectral function the thermal average is taken over both electron and phonon energies. From Eqs. (2.16) it is evident that we do not wish to take the thermal average over the electronic states. Therefore we consider only the spectral function obtained prior to the thermal averaging over the electronic energies:

$$\rho_{n_\lambda,\beta}^{(-)}(\lambda,E)=P_\beta(\lambda,-E). \quad (2.18)$$

For the simple state functions (2.13) the spectral function (2.18) can be evaluated analytically be employing Feynman's theorem[21] for disentangling operators. The result is given by

$$\rho_{n_\lambda,\beta}^{(-)}(\lambda,E)$$
$$=\frac{n_{\lambda,1}}{2\pi\hbar}\int_{-\infty}^{\infty}\exp\{i[E+E(\lambda)]t/\hbar\}g_\beta^\lambda(t)dt, \quad (2.19a)$$

$$g_\beta^\lambda(t)=\exp\left\{-\sum_{\mathbf{k}}\left|\frac{v(\mathbf{k},\lambda)}{\hbar\omega(\mathbf{k})}\right|^2\Big([1-\exp(-i\omega(\mathbf{k})t)]\right.$$
$$\left.\times[\langle n_{\mathbf{k}}\rangle+1]+[1-\exp(i\omega(\mathbf{k})t)]\langle n_{\mathbf{k}}\rangle\Big)\right\}, \quad (2.19b)$$

$$\langle n_{\mathbf{k}}\rangle=[\exp[\beta\hbar\omega(\mathbf{k})]-1]^{-1}, \quad (2.20)$$

$$E(\lambda)=E_\lambda-\Delta_\lambda. \quad (2.21)$$

We subsequently suppress the n_λ and β indices of the spectral function. The transition probability per unit time between two localized states caused by an external perturbation of the form

$$H_I=T_{\lambda_2,\lambda_1}c_{\lambda_2}^\dagger c_{\lambda_1}+\text{c.c.} \quad (2.22a)$$

is given by the similar formulas:

$$W_\beta(E)=|T_{\lambda_2,\lambda_1}|^2\hbar^{-2}F(\beta)$$
$$\times\int_{-\infty}^{\infty}\exp\{i[E+E(\lambda_1)-E(\lambda_2)]t/\hbar\}g_\beta^{\lambda_2\lambda_1}(t)dt, \quad (2.22b)$$

$$g_\beta^{\lambda_2\lambda_1}(t)=\exp\left\{-\sum_{\mathbf{k}}\left|\frac{v(\mathbf{k},\lambda_1)-v(\mathbf{k},\lambda_2)}{\hbar\omega(\mathbf{k})}\right|^2\right.$$
$$\left.\times\Big([1-\exp(-i\omega(\mathbf{k})t)][\langle n_{\mathbf{k}}\rangle+1]+[1-\exp(+i\omega(\mathbf{k})t)]\langle n_{\mathbf{k}}\rangle\Big)\right\}, \quad (2.22c)$$

[20] See, e.g., A. A. Abrikosov, L. P. Gorkov, and I. E. Pzyaloshinski, *Methods of Quantum Field Theory in Statistical Physics* (Prentice-Hall, Inc., Englewood Cliffs, New Jersey, 1963), Chap. 3.

[21] R. P. Feynman, Phys. Rev. **80**, 440 (1950); Charles Kittel, *Quantum Theory of Solids* (John Wiley & Sons, Inc., New York, 1963), pp. 393–396.

$$F(\beta)=\exp\{-\beta E(\lambda_1)/[\exp(-\beta E(\lambda_1))+\exp(-\beta E(\lambda_2))]\}. \quad (2.22d)$$

In Eqs. (2.22) the nonzero population of level 2 relative to level 1 has been neglected. These formulas are well known but the original derivations[1,4,22] utilized an expansion of $\exp(-iS_\lambda)$ which is invalid for the unshielded piezoelectric electron-phonon interaction. However, it is known that such an expansion is unnecessary to obtain Eqs. (2.22).[5,23] Our derivation of (2.19) and (2.22), requires no expansions of $\exp(-iS_\lambda)$ and no assumptions concerning the dependence of the electron-phonon vertex on the volume of the system.

In subsequent sections of this paper we obtain analytical expressions for $g_\beta^\lambda(t)$ using several electronic charge distributions $|\phi_\lambda(\mathbf{x})|^2$. The final integrations over t in (2.19a) are performed numerically on the GE 235. The new results presented herein consist of (a) the demonstration that the sums over $\mathbf{k}$ in Eqs. (2.19b) and (2.22c) can be performed analytically for continuous phonon spectra; (b) the specification of these sums for several physically interesting charge distributions, and (c) the numerical evaluation of the density of states associated with the charge distributions considered.

III. LONGITUDINAL-OPTICAL PHONONS: ARBITRARY CHARGE

The form of $W_\beta(E)$ obtained from the interaction of LO phonons with an arbitrary charge distribution was first derived by Huang and Rhys.[1] We outline a compact derivation of the known result to facilitate both the comparison of our approach to others in the literature and the comparison of the optical-mode results with those obtained for a Debye phonon spectrum. The calculation of $g_\beta^\lambda(t)$ is particularly simple because $\omega(\mathbf{k})$ is independent of $\mathbf{k}$ so that the time dependence of $g_\beta^\lambda(t)$ is independent of the charge distribution. (This convenient result ceases to be correct when the mixing of electronic states via, e.g., electron recoil, is incorporated in the dynamics.) Following the notation of Huang and Rhys we define

$$S(\lambda)\equiv\frac{1}{(\hbar\omega_l)^2}\sum_{\mathbf{k}}|v(\mathbf{k},\lambda)|^2=\frac{fq^2}{\pi\hbar\omega_l^3}\int\frac{d^3k|M_{\lambda,\lambda}(k)|^2}{k^2}, \quad (3.1)$$

in which ω_l is given by (2.6) and f by (2.8b). We obtain directly from (2.19b)

$$g_\beta^\lambda(t)=\exp\{-S(\lambda)(2n_l+1)+S(\lambda)[(n_l+1)\exp(-i\omega_l t)+n_l\exp(i\omega_l t)]\}, \quad (3.2a)$$

$$n_l\equiv[\exp(\beta\hbar\omega_l)-1]^{-1}. \quad (3.2b)$$

For $g_\beta^\lambda(t)$ given by (3.2a) the Fourier inversion can be performed analytically by expanding $g_\beta^\lambda(t)$ as a Dirichlet series.[24] We perform the expansion

$$\exp\{S(\lambda)[(n_l+1)\exp(-i\omega_l t)+n_l\exp(i\omega_l t)]\}\equiv\sum_{r=0}^{\infty}\sum_{p=0}^{\infty}\{[S(\lambda)]^{r+p}(n_l+1)^r n_l^p\times\exp[-i(r-p)\omega_l t]\}/r!p! \quad (3.3)$$

and divide the series into net emission ($r\geq p$) and net absorption ($r<p$) processes. The Fourier transform of (3.3) gives a series of delta functions whose coefficients are simply related to the power-series expansions for the modified Bessel functions $I_d(x)$.[25] The final result is the well-known formula[1,22]

$$\rho^{(-)}(\lambda,E)=\exp[-S(\lambda)(2n_l+1)]\times\sum_{d=-\infty}^{\infty}\delta(E+E(\lambda)-d\hbar\omega_l)\times\left(\frac{n_l+1}{n_l}\right)^{d/2}I_d(2S(\lambda)[n_l(n_l+1)]^{1/2}). \quad (3.4)$$

The coefficient of the delta function for a value of $d>0$ corresponds to the probability that the exact eigenstate (2.13) consists of a "bare" electron plus d optical phonons. As the exact eigenvalue is $E(\lambda)$, the "bare" electron has an energy $E(\lambda)-d\hbar\omega_l$ and more energy ($d\hbar\omega_l$) must be supplied by an external field in order to raise it to a reference state at $E=0$. In terms of the transition probability (2.22) this coefficient is interpreted as the probability that d optical phonons are created during the transition.

We are able to define a probability for the (net) emission or absorption of d phonons solely because all of the phonons have the same energy $\hbar\omega_l$. In general, the phonons exhibit a continuous energy spectrum and $\rho^{(-)}(\lambda,E)$ is interpreted as the probability that the "bare" electron coexists with an assembly of phonons whose wave vectors are unknown, but whose total energy is $E+E(\lambda)$.

Numerical calculations of the coefficients in (3.4) indicate that the phonon coexistence (emission) probabilities depend sensitively on the value of $S(\lambda)$. The maximum probability occurs when $d=[S(\lambda)]$. The major effect of increasing the temperature from 50 to 500°K is to increase the half-width of the envelope of the coefficients by a factor of about 2. The value of d associated with the maximum coexistence probability undergoes no appreciable change with temperature in the above temperature range.

[22] M. Lax, J. Chem. Phys. **20**, 1752 (1952).
[23] R. C. O'Rourke, Phys. Rev. **91**, 265 (1953); D. E. McCumber, *ibid.* **135**, A1676 (1964) and Ref. 5.
[24] B. Van der Pol and H. Bremmer, *Operational Calculus* (Cambridge University Press, Cambridge, England, 1950), p. 87.
[25] *Higher Transcendental Functions, II*, edited by A. Erdelyi (McGraw-Hill Book Company, Inc., New York, 1953), p. 85.

IV. UNSHIELDED PIEZOELECTRIC PHONONS: POINT CHARGE

The limiting case of a charged deep impurity level is a point charge. Such a charge, being localized relative to a lattice spacing, interacts strongly with all LO and LA phonons. Therefore Brillouin-zone boundary effects cut off the $\mathbf{k}$ sums in (2.19). Shallow-defect states do not couple strongly to short-wavelength phonons because their large spatial extent averages out the charge fluctuations due to these phonons. For these states the averaging alone is used to cut off the $\mathbf{k}$ sums and Brillouin zone effects are neglected. The important conclusion to be drawn from this section is that for values of E such that $E+E(\lambda)\cong 0$ the behavior of the one-electron spectral function is insensitive to the deep-shallow nature of the defect state.

The use of the Debye phonon spectrum implies that the $\mathbf{k}$ sum in (2.19b) is cut off at the maximum wave number

$$k_m=(6\pi^2 n)^{1/3} \tag{4.1}$$

in which n is the atomic density of the crystal. For a point charge at $\mathbf{x}_0$

$$M_{\lambda,\lambda}(\mathbf{k})=\exp(-i\mathbf{k}\cdot\mathbf{x}_0). \tag{4.2}$$

The point charge sets an upper bound S_m on the value of $S(\lambda)$ for the interaction of a deep defect with optical phonons.

$$S_m=4q^2 f k_m/\hbar\omega_l^3. \tag{4.3}$$

For the continuous acoustical spectrum (2.3) both the shape of the electronic charge distribution and the form of the electron-phonon vertex alter the functional form of $\rho^{(-)}(\lambda,E)$ due to the $\exp[\pm i\omega(\mathbf{k})t]$ factors in (2.19b). We study a point charge with an unshielded piezoelectric electron-phonon interaction because the long-wavelength singularity in this interaction leads to one of the most striking consequences of the phonon continuum: the existence of an "infrared catastrophe" resulting from the ease of copious emission of zero-energy phonons. At non-zero temperatures the thermal motion of the phonons prevents an actual divergence of (2.19b), but its possibility in the $\theta\to 0$ limit is reflected by a broadening and asymmetry of the zero-phonon line which is linear in θ. We find in Sec. VI that the introduction of static shielding of the interaction by mobile charge carriers yields a *bona fide* zero-phonon line but does not obliterate the low-temperature structure in the spectral function near the zero-phonon energy.

The spectral function is calculated by using (2.10a) and trigonometric identities to write (2.19b) in the form

$$g_\beta^{\lambda}(t)=\exp\left(\frac{-g}{\pi}\int_0^{k_m}\frac{dk}{k}|M_{\lambda,\lambda}(k)|^2\{i\sin(v_s kt)+[1-\cos(v_s kt)]\coth(\hbar v_s k\beta/2)\}\right) \tag{4.4}$$

in which $|M_{\lambda,\lambda}(k)|^2$ is the angular average of the form factor (2.2b). We define the dimensionless variables:

$$x=\hbar v_s\beta k_m/2, \tag{4.5a}$$

$$v=v_s k_m t, \tag{4.5b}$$

$$w=k/k_m. \tag{4.5c}$$

Introducing the variable substitution $z=iwv$ and expanding

$$\coth(x)=1+2\sum_{n=1}^{\infty}\exp(-2nx), \tag{4.6}$$

we obtain by using (4.2) and (4.5) in (4.4) the expression

$$g_\beta^{q}(t)=\exp[-gI(v,x)], \tag{4.7a}$$

$$I(v,x)=\int_0^{iv}\frac{dz}{z}[1-\exp(-z)]+2\sum_{n=1}^{\infty}\int_0^1\frac{dw}{w}[1-\cos(wv)]\exp(-2nxw). \tag{4.7b}$$

We set $\lambda=q$ to denote that (4.7) is calculated for a point charge of magnitude q. The first integral in (4.7b) can be expressed in terms of the exponential integral $E_1(iv)$.[26] The second integral is evaluated by expanding the cosine in its Taylor series about the origin, interchanging the resulting sum and integration, and utilizing an integral representation of the incomplete gamma function $\gamma(2s,2nx)$.[27] We obtain

$$I(v,x)=\gamma+\ln(iv)+S(v,x)+E_1(iv), \tag{4.8a}$$

$$S(v,x)=2\sum_{n=1}^{\infty}\sum_{s=1}^{\infty}\frac{(-)^{s+1}}{(2s)!}\left(\frac{v}{2nx}\right)^{2s}\gamma(2s,2nx), \tag{4.8b}$$

$$\gamma=0.577216\cdots. \tag{4.8c}$$

Although Eqs. (4.7) and (4.8) constitute an analytical evaluation of $g_\beta^{q}(t)$, they do not yet give a useful expression because of the nested infinite summations. In the low-temperature limit we obtain the more tractable expression

$$S(v,x)\overset{\beta\to\infty}{\to}\sum_{n=1}^{\infty}\ln(1+v^2/4n^2x^2)+O(\exp(-x)), \tag{4.9}$$

which follows from the expansion[27]

$$\gamma(n,y)=\Gamma(n)-y^{n-1}\times\exp(-y)\left[\sum_{m=0}^{N-1}\frac{(1-n)_m}{(-y)^m}+O(|y|^{-N})\right]. \tag{4.10}$$

[26] W. Gautschi and W. F. Cahill, *Handbook of Mathematical Functions* (National Bureau of Standards Applied Mathematics Series 55, Washington, D. C., 1964), p. 227.

[27] *Higher Transcendental Functions, II*, edited by A. Erdelyi (McGraw-Hill Book Company, Inc., New York, 1953), Chap. 9.

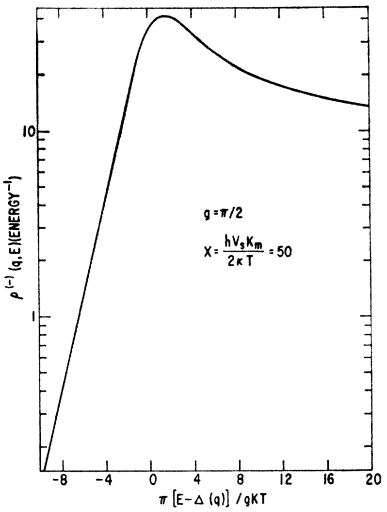

FIG. 1. The low-temperature spectral function associated with a point charge in a hypothetical strong-coupling material. Only the piezoelectric electron-phonon interaction is included in the calculation. All symbols are defined by Eqs. (4.5), (4.12), and (4.16) in the text.

The evaluation of the error estimate is not trivial and is outlined in Appendix A. Using (4.8) and (4.9) in (4.7a) and neglecting the error terms we obtain an infinite product from the sum in (4.9). This infinite product can be simply related to the hyperbolic sine[28] so we obtain the final expression:

$$g_\beta{}^q(t)=\exp\left\{\frac{-g}{\pi}[\gamma+\ln(2xi/\pi)+E_1(iv)+\ln(\sinh[\pi v/2x])]\right\}, \quad (4.11)$$

where x, v are defined in (4.5). For numerical calculations we use the identity[26]

$$E_1(iv)=i\,\mathrm{Si}(v)-\mathrm{Ci}(v)-\pi i/2,$$

in which $\mathrm{Si}(v)$ and $\mathrm{Ci}(v)$ are the exponential sine and cosine integrals which are evaluated numerically directly from their power-series expansions for $v<10$ and from their asymptotic formulas for $v\geq 10$.

If we define $\mathcal{E}_1$ as the dimensionless variable

$$\mathcal{E}_1=[E-\Delta(q)]/\hbar v_s k_m, \quad (4.12a)$$

$$\Delta(q)=g\hbar v_s k_m/\pi, \quad (4.12b)$$

we obtain for the spectral function

$$\rho^{(-)}(q,\mathcal{E}_1)=\frac{\delta_{n_q,1}}{\pi}\int_0^\infty F(v)dv, \quad (4.13a)$$

$$F(v)=\cos[\mathcal{E}_1 v-g\,\mathrm{Si}(v)/\pi]\times\exp\left\{\frac{-g}{\pi}\left[\gamma+\ln\left(\frac{2x}{\pi}\right)+\ln\left(\sinh\left[\frac{\pi v}{2x}\right]\right)-\mathrm{Ci}(v)\right]\right\}. \quad (4.13b)$$

It is easy to demonstrate that $\rho^{(-)}(q,E)$ does not exhibit a delta-function zero-phonon peak by using the asymptotic expansions[26]

$$\mathrm{Si}(v)\overset{v\to\infty}{\to}\pi/2+O(v^{-1}), \quad (4.14a)$$

$$\mathrm{Ci}(v)\overset{v\to\infty}{\to}O(v^{-1}). \quad (4.14b)$$

Thus the integrand in (4.13) exhibits the asymptotic behavior:

$$F(v)\overset{v\to\infty}{\to}\exp\left\{\frac{-g}{\pi}\left[\ln\left(\frac{x}{\pi}\right)+\gamma\right]-\frac{gv}{2x}\right\}\times\cos[\mathcal{E}_1 v-g/2]. \quad (4.15)$$

The $\exp(-gv/2x)$ term gives rise to a Lorentz-broadened analog of a zero-phonon line. The $(-g/2)$ factor in the argument of the cosine make the line asymmetric and is the origin of the Stokes' shift for the point charge.

The final form of the spectral function used for numerical evaluation is given by

$$\rho^{(-)}(q,\mathcal{E}_1)=\pi^{-1}\int_0^\infty[F(v)-F_s(v)]dv+\rho_s{}^{(-)}(q,\mathcal{E}_1), \quad (4.16a)$$

$$F_s(v)=\cos[\mathcal{E}_1 v-g/2]\exp\{-g[\ln(x/\pi)+\gamma+\pi v/2x]/\pi\}\left[1+\frac{ge^{-\pi v/x}}{\pi}+\frac{g(g+1)}{2\pi^2}e^{-2\pi v/x}\right], \quad (4.16b)$$

$$\rho_s{}^{(-)}(q,\mathcal{E}_1)=\pi^{-1}\exp\{-g[\gamma+\ln(x/\pi)]\}\sum_{n=}^{2}c_n\left\{\frac{[(g+2\pi n)/2x]\cos(g/2)+\mathcal{E}_1\sin(g/2)}{(g+2\pi n)^2/4x^2+\mathcal{E}_1{}^2}\right\}, \quad (4.16c)$$

$$c_0=1,\quad c_1=g/\pi,\quad c_2=g(g+1)/2\pi^2. \quad (4.16d)$$

The $n=0$ term in (4.16c) causes most of the structure in the analog zero-phonon line, and in the $g\to 0$ limit reduces to the zero-phonon delta function. The analog zero-phonon line consists of the superposition of a Lorentzian peak of width $(g\theta)$ and its derivative (which peaks at $\pm g\theta$) with relative weights $1:E\beta(\tan g/g)$. The shift for large values of g of the peak in the spectral

[28] See, e.g., T. J. I'a Bromwich, *An Introduction to the Theory of Infinite Series* (MacMillan and Company, London, 1955), pp. 295–296.

function to higher energies is illustrated in Fig. 1 for the case $g=\pi/2$.

We recall that the value of $\rho^{(-)}(q,E)$ represents the relative probability that the point charge coexists with a cloud of phonons whose total energy is $E-\Delta(q)$. The high-energy tail of the spectral function, evident in Fig. 1, reflects the probability that for large values of the coupling constant (g) many phonons will be created. The exponential edge of the spectral function for $E<0$ reflects the probability that the electron absorbs phonons from the thermally excited phonon bath in the crystal. This edge is a pure exponential for $E\leq[\Delta(q)-g_K T/\pi]$ as far as we calculated it (two decades), and is reminiscent of Urbach's rule for optical absorption below a band (exciton) edge.[29]

Actual materials usually exhibit smaller values of g than $\pi/2$ and the shift in the maximum of the spectral function is less evident. The zincblende semiconductor with the strongest piezoelectric coupling is ZnS for which the spectral function associated with a point charge is shown in Fig. 2. The line shape is that of $\rho_s^{(-)}(q,E)$ for $E>0.5\Delta(q)$. The exponential low-energy edge is evident for $E<0.5\Delta(q)$ as is the large high-energy tail for $E>0$. The exponential edge begins at that value of the energy at which the integrals of $[F(v)-F_s(v)]$ and $F_s(v)$ alone are approximately equal. A comparison of Figs. 2 and 3 indicates that the analog zero-phonon line exhibits the same shape for both the (deep-donor) point charge and the shallow S-wave donor.

V. S-WAVE HYDROGENIC SHALLOW DONOR WITHOUT SHIELDING

For both zincblende and Wurtzite structures most II–VI and III–V semiconductors are thought to have a minimum in an S-like conduction band at the center of the Brillouin zone.[30] Shallow donor states can be constructed[11] which are coupled to deformation potential phonons via Eq. (2.9). For shallow acceptor states, a modification of the electron-phonon coupling due to the degeneracy of the valence bands must be introduced.[31] We neglect this refinement in Sec. VII, however, and treat the hole band as possessing an equal and opposite deformation-potential constant to the electron band.

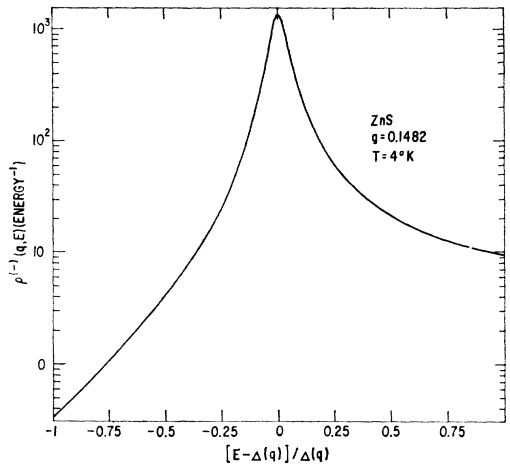

FIG. 2. The spectral function at $T=4°K$ for a point charge in ZnS. Only the piezoelectric electron-phonon interaction is incorporated in the calculation. The symbols are defined by Eqs. (4.5), (4.12), and (4.16). The selection of parameters is specified following Eq. (5.4) in the text.

The electron-phonon vertex for the shallow-donor state is taken to include the influence of both the unshielded piezoelectric interaction and the deformation-potential interaction. Because of the orthonormality of the Bloch functions at the zone center, only the effective-mass envelope function enters the Fourier transform of the charge distribution (2.2b). For an S-wave envelope we obtain

$$M_{s,s}(k)=[1+(ka_B/2)^2]^{-2}, \tag{5.1}$$

in which a_B is the Bohr radius of the impurity state and the effective charge on the impurity is taken to be the free-electron charge. The electron-phonon weighting function in (2.19b) can be written as

$$\left|\frac{v(\mathbf{k},s)}{\hbar\omega(\mathbf{k})}\right|^2=\frac{2\pi^3 g}{\Omega k^3}[\delta+\gamma k^2]|M_{s,s}(k)|^2, \tag{5.2a}$$

$$\begin{aligned}\delta&=+1\text{; piezoelectric coupling}\\&=\ 0\text{; no piezoelectric coupling,}\end{aligned} \tag{5.2b}$$

$$\gamma=D_0^2/4\pi^3\hbar v_s^3 g\rho_0. \tag{5.2c}$$

In order to perform the $\mathbf{k}$ sum in (2.19b), we replace it by an integral and use the partial-fraction expansion of the meromorphic function[28] $\coth(x)$

$$\coth(x)=\frac{1}{x}+2\sum_{n=1}^{\infty}\frac{x}{x^2+n^2\pi^2}. \tag{5.3}$$

Inserting (5.1), (5.2), and (5.3) into (2.19b), neglecting zone-boundary effects, the integral can be performed by contour-integral methods with the result:

$$g_\beta^{\,s}(t)=\exp\{-g[i\,\mathrm{sgn}(t)F(t)+I(t)]\}, \tag{5.4a}$$

$$\begin{aligned}\mathrm{sgn}(t)&=+1;\ t>0\\&=-1;\ t<0,\end{aligned} \tag{5.4b}$$

$$F(t)=\delta[1-e^{-z}]/2+\frac{e^{-z}}{96}[(\gamma k_0^2-\delta)z^3+3(\gamma k_0^2-3\delta)z^2+3(\gamma k_0^2-11\delta)z], \tag{5.4c}$$

[29] See, e.g., D. E. McCumber, Phys. Rev. 135, A1676 (1964).

[30] See, e.g., M. Cardona, *Physics of Semiconductors* (Dunod Cie, Paris, 1964), p. 181, for detailed references.

[31] W. H. Kleiner and L. M. Roth, Phys. Rev. Letters 2, 334 (1959).

$$I(t)=\delta|t|/\beta\hbar+C_1(1-e^{-z})+e^{-z}[C_2z+C_3z^2+C_4z^3]$$
$$+\frac{x^8}{\pi}\sum_{n=1}^{\infty}\left\{\frac{\delta}{n}-n\frac{\gamma k_0^2\pi^2}{x^2}\right\}$$
$$\times\frac{[1-\exp(-2\pi n|t|/\hbar\beta)]}{(x^2-n^2\pi^2)^4}, \quad (5.4d)$$

$$z=2|t|v_s/a_B, \quad (5.4e)$$

$$k_0=2/a_B, \quad (5.4f)$$

$$x=\beta\hbar v_s/a_B. \quad (5.4g)$$

The C_i are coefficients depending only upon k_0 and x. They are given in Appendix B. As in the case of the point charge, the $\delta|t|/\beta\hbar$ term in (5.4d) eliminates the zero-phonon line and replaces it by a Lorentzian of width $g\theta$. The $\delta(1-e^{-z})/2$ term in $F(t)$ contributes an asymmetry to the analog zero-phonon line.

The Fourier transform of Eqs. (5.4) is calculated, as in Sec. IV, by explicit subtraction of the large $-t$ Lorentzian form. Computations were carried out on the GE 235 using an integration accuracy of 1 part in 10^4. The calculations were made using parameters suitable for the description of three materials: ZnS, CdTe, and CdS. For the two zinc-blende materials, ZnS and CdTe, we employ the piezoelectric electron-phonon interaction given by (2.10c). The elastic constants, densities, dielectric constants, and piezoelectric constants are obtained from Berlincourt *et al.*[32] The CdTe deformation potential constant is estimated from Thomas[33] to be 3 eV. The ZnS and CdS deformation potential constants are arbitrarily set equal to 5 eV. The conduction-band effective mass for CdTe is taken from Kanazawa and Brown[34] to be $m^*=0.096m_e$ and leads to $a_B=53$ Å. No conduction-band masses have been measured for cubic ZnS. However, we do not expect the value of m^* to be excessively sensitive to the crystal structure so we use the value $m^*=0.28m_e$ given by Wheeler and Miklosz[35] for Wurtzite ZnS which leads to $a_B=15.2$ Å. For CdS we use $a_B=24$ Å, $v_s=1.8\times10^5$ cm/sec, and $g=4.1$ whose calculation is described by Hutson.[12,36]

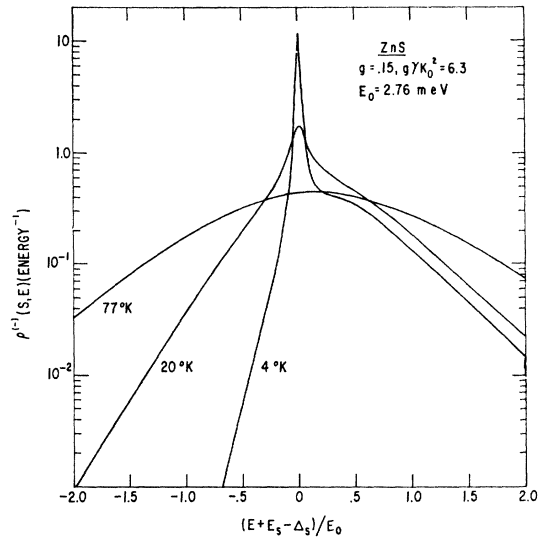

FIG. 3. The spectral functions at $T=4$, 20, and 77°K for a shallow S-wave hydrogenic donor in ZnS. The unshielded piezoelectric and deformation-potential electron-phonon interactions are included in the calculation. The symbols are defined by Eqs. (5.2), (5.4), and (2.19). The parameters are specified following Eqs. (5.4) in the text.

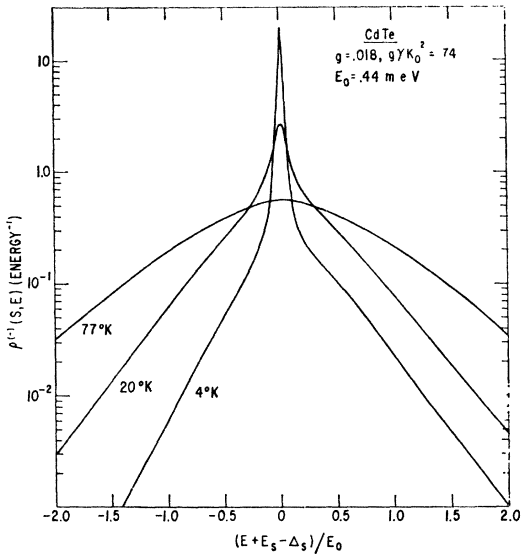

FIG. 4. The spectral functions at $T=4$, 20, and 77°K for a shallow s-wave hydrogenic donor in CdTe. The unshielded piezoelectric and deformation-potential electron-phonon interactions are included in the calculation. The symbols are defined by Eqs. (5.2), (5.4), and (2.19). The parameters are specified following Eqs. (5.4) in the text.

In ZnS and CdTe the coupling constant g assumes the values 0.148 and 0.018, respectively. Therefore they are both weakly piezoelectric in the sense that $g\ll1$. The spectral functions for each of these crystals at 4, 20, and 77°K, respectively, are shown in Fig. 3 for ZnS and Fig. 4 for CdTe. Energies are measured in units of

$$E_0=2\hbar v_s/a_B, \quad (5.5)$$

which is the uncertainty energy associated with the transit time of a sound wave across the impurity. The

[32] D. Berlincourt, H. Jaffe, and L. R. Shiozawa, Phys. Rev. **129**, 1009 (1963).

[33] D. G. Thomas, J. Appl. Phys. Suppl. **32**, 2298 (1961).

[34] K. Kanazawa and F. C. Brown, Phys. Rev. **135**, A1757 (1964).

[35] R. G. Wheeler and J. C. Miklosz, *The Physics of Semiconductors* (Dunod Cie., Paris, 1964), p. 873; R. G. Wheeler (private communication).

[36] Our value of g is found from $g=\langle k^2\rangle q^2/\epsilon(0)\hbar v_s$, where the electromechanical coupling constant $\langle k^2\rangle$ was obtained from Hutson. Only shear phonons were considered for CdS as they have the dominant interaction.

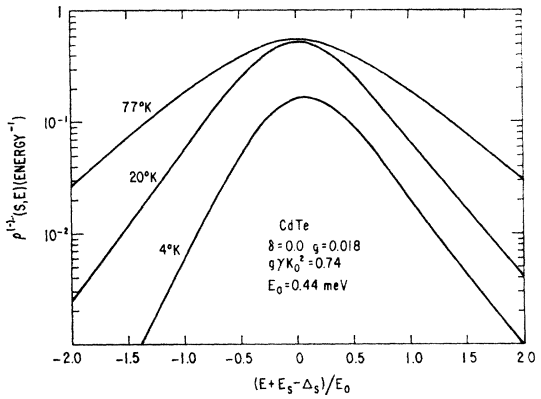

FIG. 5. The spectral functions at $T=4$, 20, and 77°K for a shallow S-wave hydrogenic donor in CdTe. Only the deformation-potential electron-phonon interaction is included in the calculation. Zero-phonon delta functions are not shown. The symbols are defined by Eqs. (5.2), (5.4), and (2.19). The parameters are specified following Eqs. (5.4) in the text.

polaron binding energy of the shallow donor state is given by

$$\Delta_s = gE_0(5\delta+\gamma k_0^2)/32. \tag{5.6}$$

For weakly piezoelectric crystals the deformation-potential electron-phonon coupling contributes more to the polaron shift and the wings of the spectral function than does the piezoelectric coupling. For ZnS and CdTe the quantity γk_0^2 is equal to 42.3 and 41.1, respectively. As $\delta=1.0$ and $\gamma=0$ gives the contribution of the piezophonons alone, we find that the deformation-potential phonons contribute about eight times as much to the polaron energy as do the piezophonons. The Lorentzian peak in the spectral function near $E=-E_s+\Delta_s$ is characteristic of the piezoelectric interaction in weakly piezoelectric crystals. It is referred to as the analog zero-phonon line and is a consequence of the k^{-3} divergence in (5.2a). The relative contributions to the spectral function due to the two kinds of phonon interactions can be seen by comparison of Fig. 4 with Fig. 5 in which the spectral functions for CdTe in the absence of piezophonon coupling are illustrated. At 77°K the spectral functions calculated with and without the piezoelectric electron-phonon interaction are identical. At the two lower temperatures, 20 and 4°K, the dominance of the deformation-potential interaction is reflected in the indistinguishability of the wings of the spectral functions calculated with and without the piezophonon interaction. In its absence the area under the analog zero-phonon line is absorbed in a *bona fide* zero-phonon delta function (not shown in Fig. 5) with the strength

$$S_0=\exp[-gL_0], \tag{5.7a}$$

$$L_0=C_1(\delta=0)-\pi\gamma k_0^2 x^6\sum_{n=1}^{\infty}\left[\frac{n}{(x^2-n^2\pi^2)^4}\right]. \tag{5.7b}$$

In ZnS, for which the piezocoupling is ten times stronger, the low-energy wing as well as the center peak is modified by the piezocoupling. However, as the deformation-potential constant for ZnS is chosen arbitrarily, the results have no quantative significance.

The emergence at low temperatures of the analog zero-phonon line of width $g\theta$ is illustrated for CdTe in Fig. 6 in which the center portion of the spectral function is shown on an energy scale of $g\theta$. This portion of the spectral function is strongly modified by the static screening of the piezoelectric interaction by mobile charge carriers. As the carrier density needed to obtain an appreciable effect is $n_q\sim 10^{+14}$ cm^{-3}, we anticipate that the center portion of the spectral function for laboratory samples is usually better represented by the results presented in the next section.

CdS, with $g=4.1$, is a strongly piezoelectric crystal. Our arbitrary selection of a deformation potential of 5 eV leads to $\gamma k_0^2=2.9$ so that the piezophonon and deformation-potential phonon contributions to the polaron shift are comparable. The piezocoupling is sufficiently strong that we no longer obtain a simple Lorentzian analog zero-phonon line but rather find a broad, shifted spectral function even at 4°K. This result is illustrated in Fig. 7 in which the spectral functions at 4°K are presented both with and without piezoelectric coupling. The extreme broadening of the wings due to the piezophonons is evident from the figure. These strong-coupling results are not discernably altered by the shielding of the piezoelectric interaction by a mobile carrier density of $n_q\sim 10^{15}$ cm^{-3}. At higher temperatures the spectral functions become still broader. This is shown in the next section for the case in which static screening is incorporated.

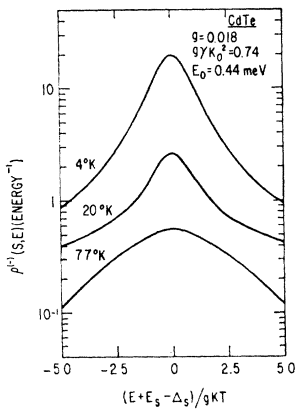

FIG. 6. The spectral functions at $T=4$, 20, 77°K for a shallow S-wave hydrogenic donor in CdTe. The energy scale is proportional to the temperature. The unshielded piezoelectric and deformation-potential electron-phonon interactions are incorporated in the calculation. The symbols are defined by Eqs. (5.2), (5.4), and (2.19). The parameters are specified following Eqs. (5.4) in the text.

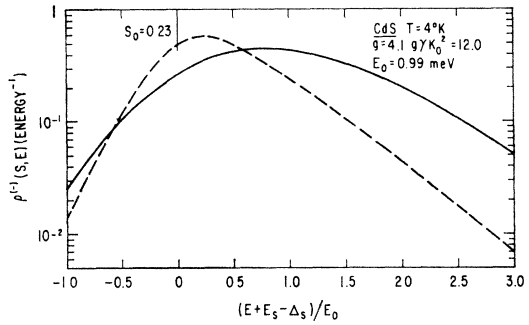

FIG. 7. Spectral functions at $T=4°K$ for a shallow S-wave hydrogenic donor in CdS. The solid line shows the spectral function calculated with both the unshielded piezoelectric and deformation-potential electron-phonon interactions. The dashed line shows the calculation using the deformation-potential interaction alone. The zero-phonon line is indicated and has the strength $S_0=0.23$. The symbols are defined by Eqs. (5.2), (5.4), (2.19), and (5.7). The parameters are specified following Eqs. (5.4) in the text.

VI. S-WAVE HYDROGENIC SHALLOW DONOR WITH SHIELDING

The static screening of the piezoelectric electron-phonon interaction by mobile charge carriers of density n_q and charge q alters the weighting function in (2.19b) from (5.2a) to

$$\left|\frac{v(k,s)}{\hbar\omega(k)}\right|^2=\frac{2\pi^3 g}{\Omega}\left[\frac{\delta k}{(k^2+k_D^2)^2}+\frac{\gamma}{k}\right]|M_{s,s}(k)|^2, \quad (6.1)$$

$$k_D^2=4\pi q^2 n_q\beta/\epsilon(0). \quad (6.2)$$

Therefore the mobile carrier screening removes the k^{-3} singularity in (5.2a) which caused the analog zero-phonon line. Equation (6.1) yields instead a *bona fide* zero-phonon line with shoulders which rise to a maximum on either side of it on the energy scale

$$E_D=rE_0, \quad (6.3a)$$

$$r=k_D a_B/2. \quad (6.3b)$$

Although the mobile-carrier density associated with a given value of r depends on the parameters of any given material, rough estimates of the carrier density may be made by noting that for the three materials discussed herein, at 4°K the value $r=0.1$ corresponds to $n_q\sim10^{15}-10^{16}$ cm^{-3}. More precisely, (6.3b) yields the formula

$$n_q=\frac{r^2\epsilon(0)T(°K)}{a_B^2(A^0)}\times1.9\times10^{18}. \quad (6.3c)$$

Carrier freeze-out can cause a spectacular rise in the height of the shoulders accompanying the zero-phonon line in weakly piezocrystals when (a) the temperature is $\sim20°K$ or lower and (b) the freeze-out mechanism reduces r below 1.0.

Using (6.1), (5.1), and (5.3) in (4.4) we perform the resulting integral by contour integration techniques (neglecting zone-boundary effects). A tedious calculation yields the result

$$g_\beta^s(t)=\exp\{-g[i\,\mathrm{sgn}(t)F(t)+I(t)]\}, \quad (6.4a)$$

$$F(t)=\delta\{[\exp(-rz)-\exp(-z)][(1+3r^2)/2(1-r^2)^5]-rz\exp(-rz)/4(1-r^2)^4\}+\exp(-z)[F_1z+F_2z^2+F_3z^3], \quad (6.4b)$$

$$I(t)=x^8\sum_{n=1}^{\infty}\left\{\left[\frac{\delta(\pi n)^3}{[(rx)^2-n^2\pi^2]^2}-\frac{\pi n\gamma k_0^2}{x^2}\right]\times\frac{[1-\exp(-2\pi n|t|/\hbar\beta)]}{[x^2-n^2\pi^2]^4}\right\}+I_1(1-e^{-rz})+I_2ze^{-rz}+I_3(1-e^{-z})+e^{-z}[I_4z+I_5z^2+I_6z^3], \quad (6.4c)$$

in which r is defined by (6.3b); z, x, and k_0 are defined in (5.4); and the coefficients F_n and I_n are given in Appendix C. From Eqs. (6.4) we see that the large $|t|$ limit of $g_\beta^s(t)$ leads to a zero-phonon line of strength

$$S_s=\exp(-gL_s), \quad (6.5a)$$

$$L_s=I_1+I_3+x^8\sum_{n=1}^{\infty}\left\{\left[\frac{\delta(\pi n)^3}{[(rx)^2-n^2\pi^2]^2}-\frac{n\pi\gamma k_0^2}{x^2}\right]\times[x^2-n^2\pi^2]^{-4}\right\}, \quad (6.5b)$$

centered at $E=-E_s+\Delta_s$ (i.e., at the bound-state energy E_s of the impurity lowered by the polaron shift). This zero-phonon line is not shown in the figures although its strength is indicated.

The primary effect of mobile-carrier shielding in weakly piezoelectric materials is the suppression of the analog zero-phonon line and the appearance of a *bona fide* zero-phonon line. This result is clearly illustrated in Fig. 8 in which the spectral functions associated with a mobile-carrier density of $n_q=1.6\times10^{13}T(°K)$ cm^{-3} are shown. A comparison of Figs. 4, 5, and 8 reveals the sensitivity of the behavior of the low-temperature spectral functions near the zero-phonon line to the existence of the piezophonon coupling and to the presence of extremely low concentrations of mobile-charge carriers. The spectral function at 77°K is essentially unaffected by either the piezophonon coupling or the presence of mobile-charge carriers.

The mobile-carrier shielding of the piezoelectric electron-phonon interaction has no appreciable effect on the wings of the spectral function. This result is evident from a comparison of Figs. 8 and 4 and also from Fig. 9 in which the spectral functions for ZnS at 4°K with various concentrations of mobile carriers

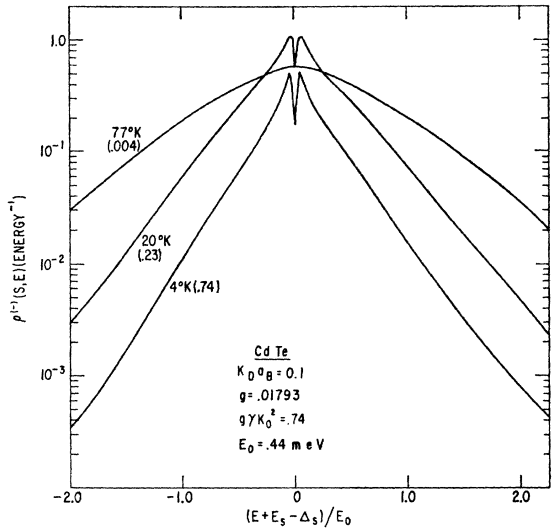

FIG. 8. Spectral functions at $T=4$, 20, and 77°K for a shallow S-wave hydrogenic donor in CdTe. The deformation-potential and shielded electron-phonon interactions are incorporated in the calculation. The symbols are defined by Eqs. (2.19), (5.4), (6.2), (6.3), (6.4), and (6.5). The numbers in parentheses associated with each spectral function are the strengths S_s of the zero-phonon lines which are not shown in the figure. The selection of parameters is specified following Eqs. (5.4) in the text.

are presented. At low carrier concentrations $k_D a_B = 0.03$ ($n_q = 6\times10^{13}$ cm^{-3}) the mobile carriers give rise to the zero-phonon-line-plus-two-shoulder structure characteristic of CdTe. However, at the higher carrier concentration $k_D a_B = 0.3$ ($n_q = 6\times10^{15}$ cm^{-3}) the low-energy shoulder is completely suppressed giving rise to a structure similar to those which will be presented in Sec. VII for excitons bound to neutral impurities.

The influence of shielding by $n_q = 7.6\times10^{12}T(°\text{K})$ cm^{-3} mobile carriers in strongly piezoelectric CdS is illustrated in Fig. 10. A comparison of Figs. 7 and 10 indicates that the shielding introduces a slightly larger slope of the wings of the spectral function and reduces the Stokes' shift of its maximum. At both 20 and 4°K the spectral functions computed with and without shielding are almost identical; a result which is reflected in part by the small strengths of the zero-phonon lines. The insignificance of the zero-phonon line in CdS contrasts sharply to its relatively large weight in the weakly piezoelectric materials. Both this result and the absence of the analog zero-phonon line without shielding are consequences of the suppression the asymptotic values of the integrands (5.4) and (6.4) relative to their value at $t=0$ for large values of the piezophonon coupling constant g.

VII. BOUND EXCITON WITHOUT SHIELDING

The spectral function of an exciton bound to a neutral defect has been discussed by Hopfield[3] using the charge-distribution form factor

$$M_{\text{BE}}(\mathbf{k}) = [1+(kr_e)^2]^{-2} - [1+(kr_h)^2]^{-2}, \quad (7.1a)$$

$$r_e = a_B(e)/2, \text{ (electron)} \quad (7.1b)$$

$$r_h = a_B(h)/2, \text{ (hole)}. \quad (7.1c)$$

This form factor neglects the Coulomb correlation between the electron and the hole, and is only useful for deformation-potential coupling when the deformation-potential constant associated with the hole band is equal in magnitude but opposite in sign to that associated with the electron band. For simplicity we assume that such is the case:

$$D_0(e) = -D_0(h) = D_0. \quad (7.2)$$

This assumption is qualitatively correct[37] but neglects effects due to the degeneracy of the valence band.[31,33,38] Using (7.2) we obtain the spectral function for the bound exciton exactly as in Sec. V but employing (7.1) instead of (5.1) in (5.2). The result is given by

$$g_\beta^{BE}(t) = \exp\{-g[i\,\text{sgn}(t)F(t)+I(t)]\}, \quad (7.3a)$$

$$F(t) = A(\delta,\gamma k_0^2,M^{-1},z)+A(\delta,\gamma M^2k_0^2,M,Mz), \quad (7.3b)$$

$$A(\delta,\gamma k_0^2,y,z) = e^{-z}(F_0+F_1z+F_2z^2+F_3z^3), \quad (7.3c)$$

$$M = m^*(h)/m^*(e), \quad (7.3d)$$

$$I(t) = I(\delta,\gamma k_0^2,x,M^{-1},z)+I(\delta,\gamma M^2k_0^2,Mx,M,Mz) + \pi^{-1}\sum_{n=1}^{\infty}\left\{\left[\frac{x^4}{(x^2-n^2\pi^2)^2}-\frac{M^4x^4}{(M^2x^2-n^2\pi^2)^2}\right] \times\left[\frac{\delta}{n}-\frac{n\gamma k_0^2\pi^2}{x^2}\right]\left[1-\exp\left(\frac{-2\pi n|t|}{\hbar\beta}\right)\right]\right\}, \quad (7.3e)$$

$$I(\delta,\gamma k_0^2,x,y,z) = I_0(1-e^{-z})+e^{-z}(I_1z+I_2z^2+I_3z^3), \quad (7.3f)$$

$$z = 2|t|v_s/a_B(e), \quad (7.3g)$$

$$k_0 = 2/a_B(e), \quad (7.3h)$$

$$x = \beta\hbar v_s/a_B(e), \quad (7.3i)$$

in which z, k_0, and x are defined as in Sec. V for the electron; M is the hole/electron mass ratio; and F_n and I_n are coefficients depending upon γk_0^2, δ, x, and y which are given in Appendix D.

The fact that the bound exciton is an electrically neutral system whereas the shallow donor (acceptor) exhibits a net (electronic) charge leads to several significant differences in the spectral functions associated with these two charge distributions. In contrast to Eqs. (5.4), Eqs. (7.3) do not yield an analog zero-phonon line. Instead the spectral function associated

[37] H. R. Phillip, W. C. Dash, and H. Ehrenreich, Phys. Rev. 127, 762 (1962).
[38] G. D. Mahan, J. Phys. Chem. Solids 26, 751 (1965).

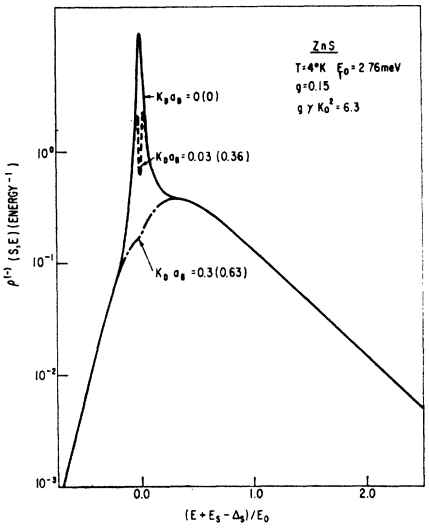

FIG. 9. Spectral functions at $T=4°$K for a shallow S-wave hydrogenic donor in ZnS. The solid line represents the spectral function calculated using the unshielded piezoelectric and deformation-potential electron-phonon interactions. The dashed lines show the spectral functions calculated using the deformation-potential and shielded piezoelectric interactions for two concentrations of mobile carriers. The symbols are defined by Eqs. (2.19), (5.2), (5.4), (6.2), (6.3), (6.4), and (6.5). The numbers in parentheses for the shielded-interaction spectral functions are the strengths S_s of the zero-phonon lines which are not shown in the figure. The selection of parameters is specified following Eqs. (5.4) in the text.

with (7.3) has the general form of a zero-phonon line of strength

$$S_0=\exp(-gL_0), \tag{7.4a}$$

$$L_0=I_0(\delta,\gamma k_0^2,x,M^{-1})+I_0(\delta,\gamma M^2k_0^2,Mx,M)$$
$$+\frac{1}{\pi}\sum_{n=1}\left\{\left[\frac{x^4}{(x^2-n^2\pi^2)^2}-\frac{M^4x^4}{(M^2x^2-n^2\pi^2)^2}\right]\times\left[\frac{\delta}{n}-\frac{n\gamma k_0^2\pi^2}{x^2}\right]\right\}, \tag{7.4b}$$

plus wings whose form depends sensitively on the relative strengths of the piezoelectric and deformation-potential electron-phonon interactions. The total polaron shift in the energy of the bound-exciton state is not simply the sum of the electron and hole polaron shifts, but is reduced by an interference term. Energies are measured in units of E_0 associated with the electron, i.e.,

$$E_0=2\hbar v_s/a_B(e) \tag{7.5}$$

and the notation $\Delta_s(g,\gamma_i^{1/2},a_B(i))$ is used for the shallow donor (acceptor) polaron shift with $i=e$, h denoting the electron and hole deformation potentials $\gamma_i^{1/2}$ and Bohr radii $a_B(i)$, respectively. For the case in which (7.2) is satisfied, i.e., $\gamma_e^{1/2}=-\gamma_h^{1/2}=\gamma^{1/2}$, the polaron shift is given by

$$\Delta_{BE}=\Delta_s(g,\gamma^{1/2},a_B(e))+\Delta_s(g,-\gamma^{1/2},a_B(h))$$
$$-gE_0\{[M(M^2+3M+1)\delta+M^3\gamma k_0^2]/2(1+M)^3\} \tag{7.6}$$

and provides an extra energy shift of the bound-exciton absorption lines relative to their free-exciton counterparts.

The charge-distribution form factor (7.1) for a bound exciton is similar to that which is to be used in Eqs. (2.22) for donor-acceptor recombination fluorescence. The weighting function in (2.22b) for these transitions depends explicitly on the separation $\mathbf{r}$ of the donor-acceptor pair. This has the interesting consequence that both the polaron shift Δ and the spectral density depend upon the value of $\mathbf{r}$. If the (S-band) donor has an S-wave form factor (5.1), then the form factor associated with a (P-band) acceptor with an S-wave envelope is given by

$$M_{s,s}^{(a)}(\mathbf{k})=\exp(-i\mathbf{k}\cdot\mathbf{r})\{1+[ka_B(h)/2]^2\}^{-2}. \tag{7.7}$$

Using the form (2.10a) for the piezoelectric electron-phonon interaction the Fourier transform of the spectral function for the recombination radiation can be calculated like the bound-exciton results presented in Eqs. (7.3). The polaron shift in the energy of the recombination radiation is given by

$$\Delta_{DA}=\Delta_s(g,\gamma^{1/2},a_B(e))+\Delta_s(g,-\gamma^{1/2},a_B(h))+gE_0\left\{-\frac{\delta}{R}+\frac{M^4}{R(1-M^2)^3}[(\delta\gamma k_0^2)^{1/2}(e^{-R}(3+M^2)-M^{-3}(3M^2+1)e^{-MR})\right.$$
$$+\delta(e^{-R}(2-M^2)+M^{-4}(1-2M^2)e^{-MR})+2\gamma k_0^2(e^{-R}-e^{-MR})]+\frac{M^4}{2(1-M^2)^2}[\gamma k_0^2(e^{-R}+e^{-MR}/M)$$
$$\left.+\delta(e^{-R}+e^{-MR}/M^3)-2(\delta\gamma k_0^2)^{1/2}(e^{-R}+e^{-MR}/M^2)]\right\}, \tag{7.8a}$$

$$R=k_0r. \tag{7.8b}$$

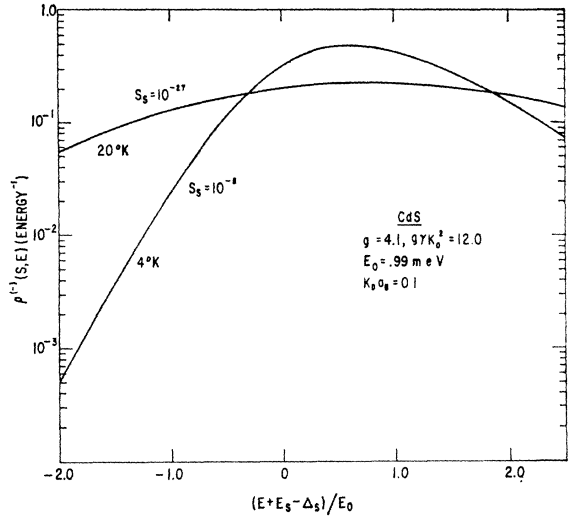

FIG. 10. Spectral functions at $T=4$ and 20°K for a shallow S-wave hydrogenic donor in CdS. The deformation-potential and shielded piezoelectric electron-phonon interactions are included in the calculation. The symbols are defined by Eqs. (2.19), (5.4), (6.2), (6.3), (6.4), and (6.5). The selection of parameters is specified following Eqs. (5.4) in the text.

The term $-gE_0\delta/R$ may be alternatively written as $-e^2\langle k^2\rangle/\epsilon(0)R$, where $\langle k^2\rangle$ is the electromechanical coupling constant, which shows that it is just the energy shift from the piezoelectric contribution to the static dielectric function.[10,39] There is no term in (7.8) which is proportional to R^{-6} because our model neglects the phonon-induced mixing of electronic states. The other R-dependent contributions to Δ_{DA} decay exponentially in the distance between the donor-acceptor pair. Finally, we note that the R^{-1} term is due directly to the infrared divergence in the electron-phonon interaction. It disappears when the shielding of the interaction by mobile charge carriers is considered, and is replaced by contributions to Δ_{DA} which decay exponentially in $k_D r$.

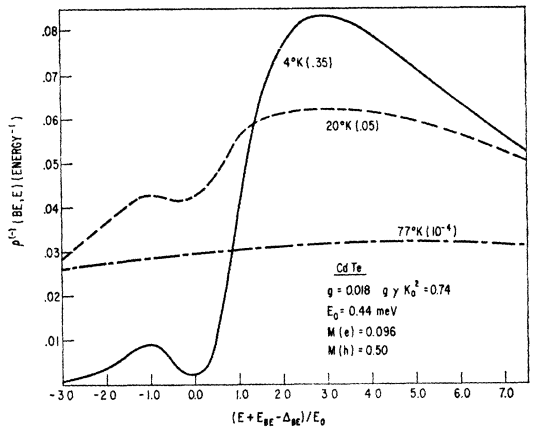

FIG. 11. Spectral functions at $T=4$, 20, and 77°K for an exciton gound to a neutral defect in CdTe. The unshielded piezoelectric and deformation-potential electron-phonon interactions are included in the calculation. The symbols are defined by Eqs. (2.19), (5.2), (7.2), (7.3), and (7.4). The hole mass is obtained from B. Segall (private communication and to be published). All other parameters are specified following Eqs. (5.4) in the text. The numbers in parentheses associated with each spectral function are the strengths S_0 of the zero-phonon lines which are not shown in the figure.

[39] See also C. Kittel, *Quantum Theory of Solids* (John Wiley & Sons, Inc., New York, 1963), p. 139 for a similar result obtained from virtual single LO phonon exchange rather than piezophonon exchange. When electron recoil is neglected, the result from second-order perturbation theory is the exact result.

The general form of the spectral function for the electrically neutral system of an exciton bound to a neutral impurity is well illustrated by Fig. 11 in which the spectral functions for CdTe are shown. The zero-phonon line at $E=-E_{BE}+\Delta_{BE}$ is not explicitly indicated in the figure. The triplet nature of the spectral function, a zero-phonon line plus two asymmetric wings, is evident. Both the asymmetry of the wings and

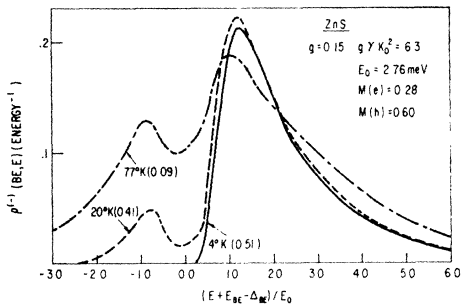

FIG. 12. Spectral functions at $T=4$, 20, and 77°K for an exciton bound to a neutral defect in ZnS. The unshielded piezoelectric and deformation-potential electron-phonon interactions are included in the calculation. The symbols are defined by Eqs. (2.19), (5.2), (7.2), (7.3), and (7.4). The hole mass is obtained from Ref. 35. All other parameters are specified following Eqs. (5.4) in the text. The numbers in parentheses associated with each spectral function are the strengths S_0 of the zero-phonon lines which are not shown in the figure.

the temperature dependence of the line shape are sensitive functions of the coupling constant g and the electron-hole mass ratio. This sensitivity is clearly visible upon comparison of Fig. 11 with Fig. 12 in which the identical calculation for ZnS are shown. The general rise in the height of the wings of the spectral function with increasing temperature accompanies a corresponding loss of strength of the zero-phonon line. For CdTe the strength of the zero-phonon line as a function of temperature is shown in Fig. 13. Surprisingly, the temperature dependence is a pure exponential in κT not only above the Debye temperature but down to 15°K. The CdTe results in Fig. 11 clearly reveal that with increasing temperature not only is the low-energy wing raised in magnitude, but the entire spectral function is broadened until at 77°K no trace of the low-temperature structure remains.

The distinction between the spectral functions associated with weakly and strongly piezoelectric materials is less pronounced for the neutral bound excitons

than for the charged donors. The spectral functions for CdS, shown in Fig. 14, exhibit qualitative similarity to the CdTe ones. The rather large difference between our results and those of Hopfield[3] results from the inclusion of the deformation-potential electron-phonon interaction. In the absence of the deformation-potential electron-phonon interaction we recover results similar to those of Ref. 3. A numerical comparison of the two results is not possible because the parameters used in computing the figures in Ref. 3 are not given.

From Figs. 11, 12, and 14 we conclude that the model charge distribution Eqs. (7.1) leads to spectral functions which exhibit qualitatively the same behavior as the experiment results.[10,40] From Eqs. (2.22) we see that these spectral functions also should describe qualitatively the phonon-induced modifications of the transition probability for transitions within the levels of a single charged donor (acceptor). Langer and Ibuki[9] have measured a three-pronged spectral function for the transitions between the Mn^{++} states of $ZnS:Mn^{++}$. In order to perform a detailed analysis of such relatively deep donor states one must have as input information the wave functions (i.e., charge distributions) of the impurity states in a frozen lattice. Once these wave functions are known, the analysis described herein can be applied to describe the phonon-induced broadening of the spectra associated with any point defect.

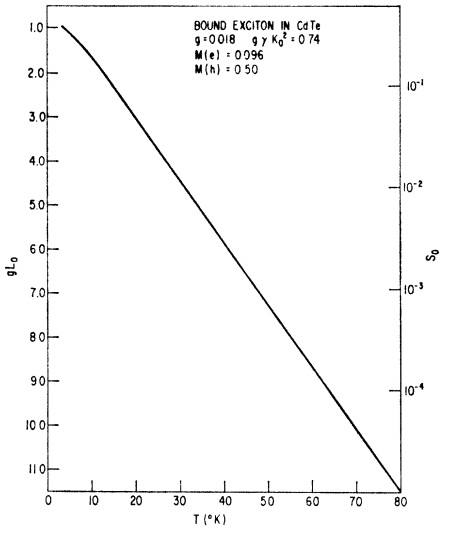

FIG. 13. The strength of the zero-phonon line associated with an exciton bound to a neutral defect in CdTe. The unshielded piezoelectric and deformation-potential electron-phonon interactions are included in the calculation. The symbols are defined by Eqs. (5.2), (7.2), (7.3), and (7.4). The hole mass is obtained from J. J. Hopfield and D. G. Thomas [Phys. Rev. **122**, 35 (1961)]. All other parameters are specified following Eqs. (5.4) in the text.

[40] D. G. Thomas and J. J. Hopfield, Phys. Rev. **128**, 2153 (1962).

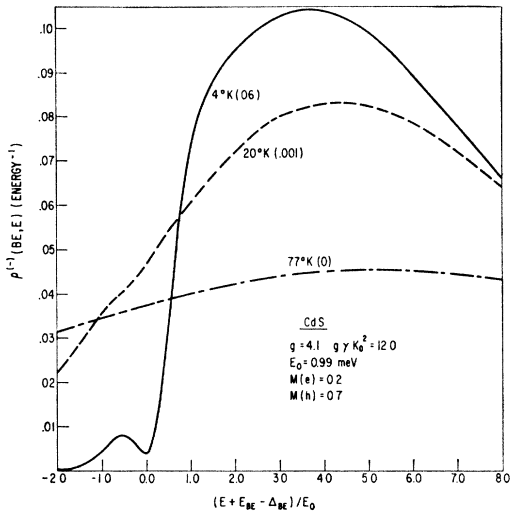

FIG. 14. Spectral functions at $T=4$, 20, and 77°K for an exciton bound to a neutral defect in CdS. The unshielded piezoelectric and deformation-potential electron-phonon interactions are included in the calculation. The symbols are defined by Eqs. (2.19), (5.2), (7.2), (7.3), and (7.4). The hole mass is obtained from J. J. Hopfield and D. G. Thomas [Phys. Rev. **122**, 35 (1961)]. All other parameters are specified following Eqs. (5.4) in the text. The numbers in parentheses associated with each spectral function are the strengths S_0 of the zero-phonon lines which are not shown in the figure.

VIII. DISCUSSION

We have evaluated the density of states $\rho^{(-)}(\lambda,E)$ at finite temperatures for a number of simple yet relevant impurity states in solids. The density of states may be expressed as the Fourier transform of $g_\beta^\lambda(t)$ given by (2.19b). When calculating the effects of acoustical and optical phonons on $\rho^{(-)}(\lambda,E)$, the general formula (2.19) for evaluating $g_\beta^\lambda(t)$ is known. Also, the evaluation (3.4) of $g_\beta^\lambda(t)$ and $\rho^{(-)}(\lambda,E)$ for optical phonons is well known. Our main purpose here is to point out that $g_\beta^\lambda(t)$ may also be found exactly for acoustical phonons interacting with simple impurity states encountered in semiconductors.

To illustrate the nature of the results, we have found $g_\beta^\lambda(t)$ for four impurity states: point charge, hydrogenic donor (or acceptor) without Debye screening, hydrogenic donor with Debye screening, and an exciton bound to a defect. In all cases the expressions for $g_\beta^\lambda(t)$ were sufficiently complicated that the density of states $\rho^{(-)}(\lambda,E)$ had to be obtained by numerical integration. Yet the exact expressions for $g_\beta^\lambda(t)$ do allow two quantities of experimental interest to be expressed exactly: the temperature-independent polaron shift Δ, and the temperature-dependent height of the zero-phonon line.

It was found that the height (spectral weight) of the zero-phonon line can be accurately represented by

$$\exp(-T/T_1) \tag{8.1}$$

down to very low temperatures. The exact form of T_1 is very complicated, and, of course, depends upon the

defect. But (8.1) appears valid down to 15°K, and deviations from this form are small at even lower temperatures.

When the Debye screening from free carriers is unimportant, neither the point charge nor the hydrogenic donor density of states have a zero-phonon line. This arises from the piezoelectric coupling of these states to long-wavelength phonons. The zero-phonon line arises when there is a finite probability of the electronic state not being coupled to any phonons at any given time. But when coupling is allowed to long-wavelength phonons, which can have vanishingly small energies, this probability goes to zero. Instead, the center of the density of states is dominated at low temperatures by a Lorentzian peak of width $g\kappa T$. This interesting physical result can only be deduced by finding $g_\beta^\lambda(t)$ exactly. The Lorentzian behavior is the result of processes involving many phonons, and would be difficult to obtain by perturbation theory.

The effect of free carriers is to screen out the electronic coupling to the long-wavelength phonons. This will cause the density of states to now have a zero-phonon line. The relevant parameter for the hydrogenic donor is $r=k_D a_B/2$ which is proportional to the square root of the mobile charge density. When $r\to 0$ there is a Lorentzian, and, when r is large, there is a strong zero-phonon line. As shown in Sec. VI, intermediate values of r give rise to unusual behavior in the density of states. Thus the density of states of a donor is sensitively dependent upon the density of mobile charges in the lattice. This result leads to the rather unusual consequence that removing impurities from a solid, which reduces the mobile charge-carrier density, broadens rather than sharpens the density of states near the zero-phonon line.

The experimentalist is interested in measurable results such as theoretical optical-absorption spectra. Our calculated density of states for the point charge and for the donor are not simply related to optical spectra. In optical absorption (or fluorescence) of donors, an electron is taken from (or dropped into) the valence band. The calculation of optical spectra must involve averaging over the valence band density of states and thermal occupation, which is also altered by phonon interactions. Yet it is clear that in the averaging procedure the most important part of the donor density of states is just the Lorentzian and zero-phonon structure. The remaining wings will just contribute background. Our formulas for the temperature-dependent spectral weight of the Lorentzian zero-phonon structure do provide direct information on the possible observation of these donor spectra.

The results of Sec. VII for the exciton bound to a defect are much more directly related to optical-absorption spectra. Indeed, the calculated $\rho^{(-)}(\lambda,E)$ is directly proportional to absorption or emission spectra. Our exact formulas for $g_\beta^\lambda(t)$ allows $\rho^{(-)}(\lambda,E)$ to be evaluated and compared directly with experiments. Our sample calculations show that $\rho^{(-)}(\lambda,E)$ has a strong dependence upon the ratio of electron and hole masses. This is unfortunate in view of our simplifying assumptions concerning the hole mass. We assume that the valence band was nondegenerate and parabolic, whereas most semiconductors have degenerate valence bands characterized by several parameters. Since a more realistic calculation is intractable, our results are still quite useful in understanding the nature of these optical spectra.

ACKNOWLEDGMENTS

We wish to thank E. Kreiger for assisting in the numerical computations and Dr. D. Langer for providing a copy of his paper prior to its publication.

APPENDIX A: ERROR ESTIMATES FOR THE POINT CHARGE

In this Appendix we outline the estimation of the error terms in (4.9). These terms come from two sources: the use of only the leading term of (4.10) in (4.8) and the fact that if $v>1$ the power series in (4.8) diverges and can only formally be summed to give a logarithm. We consider both sources of error simultaneously by observing that $\gamma(2s,2nx)=(0.95)\Gamma(2s)$ when $nx=10s/7\cong s$. Thus when $n\geq s/x$ we make errors of at most 5% by replacing $\gamma(2s,2nx)$ by $\Gamma(2s)$. However, when $n<s/x$, the use of only the leading term in (4.10) is unjustified. To estimate our errors in this case we use the small nx expansion[27] $\gamma(2s,2nx)\cong e^{-2nx}(2nx)^{2s}/2s$. The region which is cross hatched in Fig. 15 shows the region of

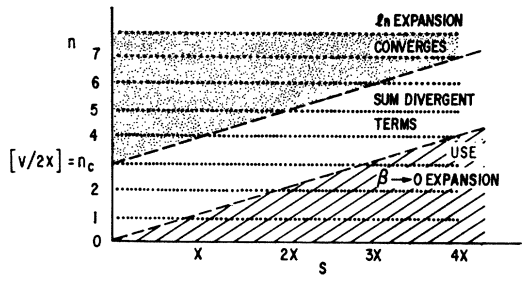

FIG. 15. A schematic diagram of the n-s plane over which the summations in Eqs. (4.8b) and (A1) are treated by using different approximations. The symbols are defined in Appendix A.

the n-s plane in which we use this expansion. We next write (4.8b) as

$$S(v,x)=\sum_{n=1}^{\infty} S_n(v,x), \tag{A1a}$$

$$S_n(v,x)\cong\sum_{s=1}^{nx}\frac{(-)^{s+1}}{s}\left(\frac{v}{2nx}\right)^{2s}+\sum_{s=nx}^{\infty}e^{-2nx}\frac{(-)^{s+1}}{(2s)!(2s)}v^{2s}. \tag{A1b}$$

The sum in the last term is completed and the resulting power series is related to $\mathrm{Ci}(v)$ by a standard expansion.[26] The terms added into the first term are bounded by

$$\frac{e^{-2nx}}{2(2s)!}\leq\frac{1}{2e}\left(\frac{1}{2nx}\right)^{2s}$$

with the equality occurring at $s=nx$: the last term in the first series. Thus the errors incurred by neglecting the added terms to the first series are of the same order as those incurred by our limiting expressions for $\gamma(2s,2nx)$ and will be ignored. The final result is

$$S_n(v,x)\cong\sum_{s=1}^{nx}\frac{(-)^{s+1}}{s}\left(\frac{v}{2nx}\right)^{2s}+(\gamma+\ln v-\mathrm{Ci}(v))e^{-2nx}. \quad \text{(A2)}$$

We found in Eq. (4.15) that it was the term resulting from replacing the sum in (A2) by a logarithm which gave the Lorentzian broadening of the "analog zero-phonon" line. We subsequently confine our attention to estimating (A1) and (A2) in the large v limit in order to verify that our use of (4.9) in (4.8b) does not lead to a spurious result. In this limit, using (4.14b) Eq. (A2) becomes

$$S_n(v,x)\overset{v\gg1}{\rightarrow}\sum_{s=1}^{nx}\frac{(-)^{s+1}}{s}\left(\frac{v}{2nx}\right)^{2s}+e^{-2nx}\ln v. \quad \text{(A3)}$$

Case I: $2x>v\gg1$: The sum consists of the first nx terms of a convergent power series for $\ln(1+\pi^2v^2/4x^2)$ and we obtain the bound for the largest error (obtained when $n=1$).

$$\left|S_1(v,x)-\ln\left[1+\left(\frac{\pi v}{2x}\right)^2\right]\right|\leq|e^{-2x}\ln v|+\left|\sum_{s=x}^{\infty}\frac{(-)^{s+1}}{s}\left(\frac{v}{2x}\right)^{2s}\right|\leq|e^{-2x}\ln(2x)|+x^{-1}(v/2x)^{2x}/[1+(v/2x)^2] \quad \text{(A4)}$$

which can be made arbitrarily small for a fixed value of v by increasing x.

Case II: $v>2x\gg1$: In this case the power series in (A3) represents the first terms of a convergent logarithmic expansion only for values of $n>n_c=[v/2x]$. We therefore sum explicitly those terms in the unshaded region of the $n-s$ plane in Fig. 15 along diagonal lines parallel to those shown in the figure. Labeling the value n at which the diagonal line begins by $\alpha+1$, the contribution of the terms in the unshaded region is bounded by

$$\sum_{\alpha=0}^{n_c-1}\sum_{s=1}^{x}\left|\sum_{n=s}^{\infty}\frac{(-)^{n+1}}{n}\left[\frac{v/2}{n-s+x(\alpha+1)}\right]^{2n}\right|\leq\sum_{\alpha=0}^{n_c-1}\sum_{s=1}^{x}\left|\frac{(-)^{s+1}}{s}\left(\frac{v}{2x(\alpha+1)}\right)^{2s}\exp(-v^2/4)\right|\leq\exp(-v^2/4)\frac{[(v/2x)^{2(x-1)}-1]}{1+(2x/v)^2}$$

$$\times\sum_{\alpha=0}^{n_c-1}\frac{1}{(\alpha+1)^2}\leq\exp(-v^2/4)\zeta(2)\left[\frac{(v/2x)^{2(x-1)}-1}{1+(2x/v)^2}\right]\overset{v\gg2x\gg1}{\longrightarrow}\exp(-v^2/4)\zeta(2)\times\left(\frac{v}{2x}\right)^{2(x-1)}, \quad \text{(A5)}$$

where $\zeta(s)$ is the Riemann zeta function.[41] Maximizing $v^{2x}\exp(-v^2/4)$ we obtain from (A1), (A2), and (A5)

$$S(v,x)\overset{v>2x\gg1}{\longrightarrow}\sum_{n=n_c+1}^{\infty}\sum_{s=1}^{(n-n_c)2x}\frac{(-)^{s+1}}{s}\left(\frac{v}{2nx}\right)^{2s}+e^{-2x}\ln v+R(v,x) \quad \text{(A6a)}$$

$$R(v,x)<(1.645)e^{-x}(2x)^{-x}. \quad \text{(A6b)}$$

Equations (A6) are the basis for the error estimates given in Eqs. (4.9). The $\ln v$ term in (A6) is slowly varying relative to the linear term in (4.15) and hence does not spoil the Lorentzian broadening of the analog zero-phonon line.

APPENDIX B: SPECTRAL FUNCTION COEFFICIENTS WITHOUT MOBILE-CARRIER SCREENING

The coefficients used in Eqs. (5.4) are given by

$$C_1=-\tfrac{1}{32}[16\delta\cot x+(11\delta-\gamma k_0^2)x\csc^2x+2(3\delta-\gamma k_0^2)\times x^2\cot x\csc^2x+\tfrac{2}{3}(\delta-\gamma k_0^2)x^3(3\cot^2x+1)\csc^2x], \quad \text{(B1)}$$

$$C_2=\tfrac{1}{32}[(11\delta-\gamma k_0^2)\cot x+2(3\delta-\gamma k_0^2)x\csc^2x+2(\delta-\gamma k_0^2)x^2\cot x\csc^2x], \quad \text{(B2)}$$

$$C_3=\tfrac{1}{32}[(3\delta-\gamma k_0^2)\cot x+(\delta-\gamma k_0^2)x\csc^2x], \quad \text{(B3)}$$

$$C_4=(1/96)(\delta-\gamma k_0^2)\cot x. \quad \text{(B4)}$$

All symbols are defined in the text.

[41] *Higher Transcendental Functions I*, edited by A. Erdelyi (McGraw-Hill Book Company, Inc., New York, 1953), Chap. 1.

APPENDIX C: SPECTRAL-FUNCTION COEFFICIENTS WITH MOBILE-CARRIER SCREENING

It is convenient to define $R=(1-r^2)^{-1}$, in terms of which the coefficients of Eq. (6.4) may be written as

$$F_1=\gamma k_0^2/32+(\delta/32)(R^2+12R^3-24R^4),$$

$$F_2=\gamma k_0^2/32+(\delta/32)(R^2-4R^3),$$

$$F_3=(\gamma k_0^2-\delta R^2)/96,$$

$$I_1=(\delta/4)\{8R^5\cot(xr)-R^4[6\cot(xr)+xr\csc^2(xr)]\},$$

$$I_2=\delta(rR^4/4)\cot(xr),$$

$$I_3=(\gamma k_0^2/32)[x\csc^2x+2x^2\cot x\csc^2x+\tfrac{2}{3}x^3(3\cot^2x+1)\csc^2x]-(\delta/96)[192R^5\cot x-72R^4(2\cot x-x\csc^2x)$$
$$-12R^3(3x\csc^2x-2x^2\csc^2x\cot x)-R^2(3x\csc^2x+6x^2\csc^2x\cot x-2x^3(3\cot^2x+1)\csc^2x)],$$

$$I_4=-(\gamma k_0^2/32)[\cot x+2x\csc^2x+2x^2\cot x\csc^2x]+(\delta/32)[24R^4\cot x-4R^3(3\cot x-2x\csc^2x)$$
$$-R^2(\cot x+2x\csc^2x-2x^2\csc^2x\cot x)],$$

$$I_5=-\gamma k_0^2(\cot x+x\csc^2x)+(\delta/32)[4R^3\cot x-R^2(\cot x-x\csc^2x)],$$

$$I_6=[(\delta R^2-\gamma k_0^2)/96]\cot x.$$

All symbols are defined in the text.

APPENDIX D: SPECTRAL-FUNCTION COEFFICIENTS FOR THE BOUND EXCITON

The coefficients used in Eqs. (7.3) of the text are given by

$$F_0=-\delta/2+(1-y^2)^{-3}[(1-3y^2)\delta+2\gamma k_0^2y^2],$$

$$F_1=\frac{\gamma k_0^2-11}{32}+\frac{\delta-\gamma k_0^2}{2(1-y^2)^2},$$

$$F_2=(\gamma k_0^2-3\delta)/32,$$

$$F_3=(\gamma k_0^2-\delta)/96,$$

$$I_0=[-\delta/2+\delta/(1-y^2)^2-2y^2(\delta-\gamma k_0^2)/(1-y^2)^3]\cot x+[(\gamma k_0^2-11\delta)/32+(\delta-\gamma k_0^2)/2(1-y^2)^2]x\csc^2x$$
$$+(\gamma k_0^2-3\delta)x^2\csc^2x\cot x/16+(\gamma k_0^2-\delta)x^3\csc^2x(3\cot^2x+1)/48,$$

$$I_1=[(11\delta-\gamma k_0^2)/32+(\gamma k_0^2-\delta)/2(1-y^2)^2]\cot x+(3\delta-\gamma k_0^2)x\csc^2x/16+(\delta-\gamma k_0^2)x^2\csc^2x\cot x/16,$$

$$I_2=(3\delta-\gamma k_0^2)\cot x/32+(\delta-\gamma k_0^2)x^2\csc^2x\cot x/16,$$

$$I_3=(\delta-\gamma k_0^2)\cot x/96.$$

All symbols are defined in the text.

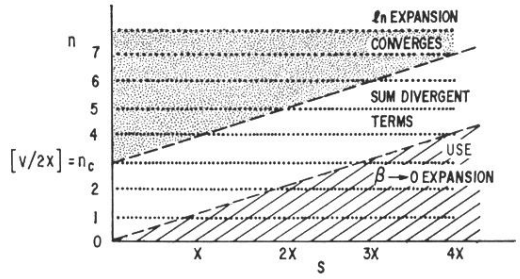

FIG. 15. A schematic diagram of the *n-s* plane over which the summations in Eqs. (4.8b) and (A1) are treated by using different approximations. The symbols are defined in Appendix A.